Available online at www.sciencedirect.com
SCIENCE DIRECT®
Journal of Solid State Chemistry 170 (2003) 294–302
JOURNAL OF SOLID STATE CHEMISTRY
http://elsevier.com/locate/jssc

An XRPD *ab-initio* structural determination of La_2RuO_5

Philippe Boullay,[a,*] D. Mercurio,[a] A. Bencan,[b] A. Meden,[c] G. Drazic,[b] and M. Kosec[b]

[a] *Science des Procédés Céramiques et de Traitements de Surface, CNRS - UMR6638, Université de Limoges, Faculté des Sciences, 123 Av. Albert Thomas, 87060 Limoges Cedex, France*
[b] *Josef Stefan Institute, Jamova 39, Ljubljana 1000, Slovenia*
[c] *Faculty of Chemistry and Chemical Technology, Askerceva 5, 1000 Ljubljana, Slovenia*

Received 20 June 2002; received in revised form 18 September 2002; accepted 24 September 2002

Abstract

The crystal structure of a new oxide, La_2RuO_5, was determined ab initio using conventional laboratory X-ray powder diffraction. Combining X-ray and electron diffraction techniques, we found that the new phase crystallized in the monoclinic system with the space group $P2_1/c$ (SG no.14) and the cell parameters $a=9.1878(2)$ Å, $b=5.8313(2)$ Å, $c=7.9575(2)$ Å and $\beta=100.773(2)°$ ($V=418.8$ Å^3, $Z=4$). The structural determination with the Patterson method and Fourier difference syntheses and the final Rietveld refinement were performed by means of the JANA2000 program. The structure is built up from the regular stacking of a two octahedra thick $[LaRuO_4]_\infty$ zigzag perovskite slab and an original $\sim$3.4 Å thick $[LaO]_\infty$ slab which constitutes the key feature of this new structure.

Keywords: Crystal structure; Lanthanum ruthenate; Layered compounds

1. Introduction

At present, the operating temperature of solid-oxide fuel cells (SOFCs) is around 1000°C; however, the next generation of SOFCs will have lower operating temperatures, of around 800°C. For an SOFC operating at 1000°C, the cathode (air electrode) materials are usually based on $(La_{1-x}Sr_x)MnO_3$. This material is a relatively good electronic conductor (resistivity 0.1 Ω cm at 1000°C) but its ionic conductivity is low; at lower operating temperatures, the polarization losses of manganites are too high for the efficient operation of an SOFC. Therefore, other materials with potentially better electrical characteristics are being investigated. These include RuO_2 and electrically conducting ruthenates, which are known to be promising electrocatalysts for oxygen reduction.

Nine compounds were synthesized in the system La–Ru–O: α-La_3RuO_7 [1], β-La_3RuO_7 [2], $La_{4.87}Ru_2O_{12}$ [3], $La_7Ru_3O_{18}$ [3], $La_8Ru_4O_{21}$ [4], $La_3Ru_3O_{11}$ [5], $LaRuO_3$ [6–8], $La_{3.5}Ru_4O_{13}$ [9] and $La_4Ru_6O_{19}$ [10]. Only $La_{3.5}Ru_4O_{13}$, $La_{4.87}Ru_2O_{12}$, $La_7Ru_3O_{18}$ and La_3RuO_7 have been prepared in air while others have been synthesized under reducing or strongly oxidizing conditions. In course of a systematic investigation of this system, we have evidence the existence of a new oxide with the nominal composition La:Ru = 2:1. X-ray absorption methods, extended X-ray absorption fine structure (EXAFS), and X-ray absorption near edge structure (XANES), were performed, which provided first structural information on the new compound [11]. The remarkable finding was that the formal Ru valency was +4 leading to an estimated composition of La_2RuO_5. Results of electrical DC resistance showed that this new phase is a conductor at room temperature ($\sim$100 Ω cm). These results as well as the compatibility studies of La_2RuO_5 with electrolyte-based materials will be published elsewhere.

In this paper, we report the crystal structure determination of the new oxide La_2RuO_5, based on a combination of results obtained from selected area electron diffraction (SAED) and X-ray powder diffraction (XRPD). The structural characteristics of the new compound will be discussed.

*Corresponding author. Fax: +33-5-55-45-72-70.
E-mail address: Philippe.Boullay@unilim.fr (P. Boullay).

0022-4596/03/$ - see front matter © 2002 Elsevier Science (USA). All rights reserved.
PII: S0022-4596(02)00088-9

2. Experimental

The polycrystalline sample of La_2RuO_5 was synthesized from $La(OH)_3$ (Ventron, 99.9%) and RuO_2 (Ventron, 99.9%). Stoichiometric amounts of the oxides were mixed in isopropyl alcohol, pressed into pellets and then fired in air at 1150°C for 60 h with intermediate grinding. During firing the pellets were placed on platinum foils.

The chemical composition of powder was analyzed using inductively coupled plasma optical emission spectroscopy (ICP-OES) for the La and Ru content, and with IR spectroscopy in the case of oxygen. These analyses indicated that the weight percent of La, Ru and O were $57.4\pm2.9\%$, $21.7\pm1.1\%$ and $18.04\pm0.45\%$, respectively. These results combined with the XANES study [11] allowed us to consider with confidence that the chemical composition of the new phase was La_2RuO_5.

The XRPD pattern used for the structural determination was recorded in the 2θ range of 12°–122° with a 0.02° step (counting time: 40 s per step) using a Siemens D5000 diffractometer ($CuK\alpha_1/K\alpha_2$—Graphite monochromator).

SAED patterns were obtained with a JEOL 100CX2 microscope operating at 100 kV and using a tilting–rotating sample holder. For the SAED experiments, the powder was crushed in an agate mortar to obtain small fragments that were put in a suspension in alcohol. A drop of the suspension was then deposited and dried on a copper grid previously coated with a thin film of amorphous carbon.

3. Cell parameters and space group assignment

The position of the main diffraction peaks were extracted from the XRPD patterns and indexed using the TREOR program [12]. A monoclinic unit cell (unique axis b) with $a\sim9.18$ Å, $b\sim5.8$ Å, $c\sim3.97$ Å and $\beta\sim100.8°$ was found to be consistent with the selected peaks. In order to check this solution, the reciprocal space of the new phase was investigated with

Table 1
Refined structural parameters for La_2RuO_5 ($Z=4$): $R_F=2.7\%$, $R_{wp}=10.8\%$ and $\chi^2=3.5$ (number of independent parameters: 52) Space group $P2_1/c$ (no. 14) with $a=9.1878(2)$ Å, $b=5.8313(2)$ Å, $c=7.9575(2)$ Å and $\beta=100.773(2)°$ ($V=418.8$ Å^3)

Atom	Wyckoff site	x	y	z	U_{iso}
La(1)	4*e*	0.16911(15)	0.2496(6)	0.0382(2)	0.0119(5)
La(2)	4*e*	0.55247(16)	0.2623(6)	0.3791(2)	0.0116(6)
Ru	4*e*	0.8505(2)	0.2522(9)	0.2115(4)	0.0095(5)
O(1)	4*e*	0.2838(15)	0.015(3)	0.780(2)	0.011(2)
O(2)	4*e*	0.3178(14)	−0.021(3)	0.376(2)	0.011(2)
O(3)	4*e*	0.9821(13)	−0.053(4)	0.712(2)	0.011(2)
O(4)	4*e*	0.8430(18)	0.169(2)	0.959(2)	0.011(2)
O(5)	4*e*	0.4297(18)	0.159(3)	0.099(2)	0.011(2)

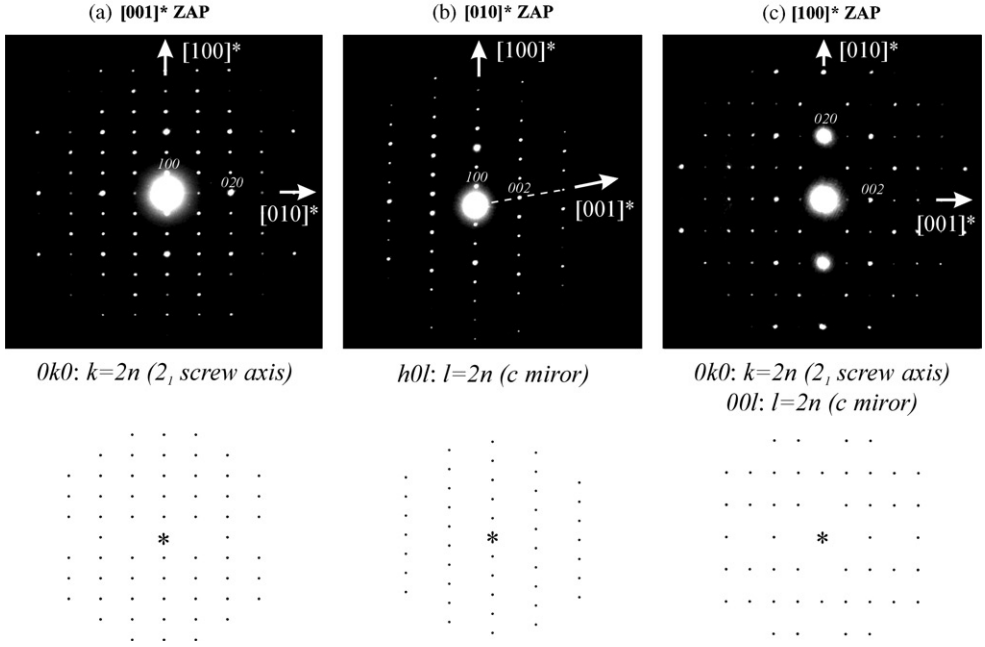

Fig. 1. SAED patterns observed for the (a) [001]*, (b) [010]* and (c) [100]* zone axis patterns. Below each experimental ZAPs, the extinction conditions are indicated together with the simulated patterns associated to these conditions. In (a) and (c), spots corresponding to *0k0: k=2n+1* and *00l: l=2n+1* are observed because of multiple scattering of the diffracted beams.

Table 2
Selected bond distances (Å) and angles (°) for La_2RuO_5

La(1)	–O(1)	2.831(18)	O(1)	–O(2)	2.98(3)
	–O(1)	2.436(17)		–O(3)	2.752(18)
	–O(2)	2.586(19)		–O(4)	2.78(2)
	–O(3)	2.87(2)		–O(4)	2.87(2)
	–O(3)	2.485(18)		–O(5)	2.77(2)
	–O(3)	2.98(2)		–O(5)	2.82(2)
	–O(4)	2.982(16)		–O(5)	2.86(2)
	–O(4)	2.443(17)	O(2)		
	–O(5)	2.410(17)		–O(3)	2.747(18)
				–O(4)	2.93(2)
La(2)	–O(1)	2.682(19)		–O(4)	2.81(2)
	–O(1)	2.770(16)		–O(5)	2.81(2)
	–O(2)	2.713(17)		–O(5)	2.95(2)
	–O(2)	2.514(18)		–O(5)	2.82(2)
	–O(2)	2.838(19)	O(3)		
	–O(4)	2.656(16)		–O(3)	2.98(3)
	–O(5)	2.381(17)		–O(3)	2.98(3)
	–O(5)	2.33(2)		–O(4)	2.85(2)
	–O(5)	2.30(2)		–O(4)	2.89(2)
Ru				–O(4)	2.80(2)
	–O(1)	2.00(2)	O(5)		
	–O(2)	2.055(17)		–O(5)	2.89(2)
	–O(3)	1.934(17)			
	–O(3)	2.13(2)			
	–O(4)	2.058(18)			
	–O(4)	2.034(18)			
Ru	–O(1)–O(2)	94.8(7)	Ru	–O(2)–O(4)	91.4(7)
	–O(1)–O(3)	88.9(7)		–O(3)–O(3)	94.4(7)
	–O(1)–O(4)	86.6(7)		–O(3)–O(4)	92.7(7)
	–O(1)–O(4)	90.6(7)		–O(3)–O(4)	89.9(7)
	–O(2)–O(3)	82.0(7)		–O(3)–O(4)	96.3(7)
	–O(2)–O(4)	86.2(7)		–O(3)–O(4)	86.3(7)

SAED. It is clear that the phase crystallizes in a monoclinic form and thus only tilting experiments around the [010]* axis can be used for a three-dimensional (3D) reconstruction of the reciprocal space. From this reconstruction, extra diffraction spots were observed in comparison with the above-mentioned cell and it is necessary to consider a doubling of the c parameter to index the observed SAED patterns properly. The determined unit-cell parameters were $a \sim 9.18$ Å, $b \sim 5.8$ Å, $c \sim 7.94$ Å and $\beta \sim 100.8°$.

Regarding the rules for systematically absent reflections obtained from the SAED patterns, no systematic absence over $h\,k\,l$ was observed and so we assumed that the lattice symbol of the space group was P. While tilting around the [010]* axis, a systematic extinction was observed for the $0\,k\,0$ row of reflection corresponding to the existence of the condition $0\,k\,0$: $k=2n$. Examining the [010]* zone axis patterns (ZAPs), the systematic extinction $h\,0\,l$: $l=2n+1$ gives the space group $P2_1/c$ (SG no. 14) as the unique solution. The [001]*, [010]* and [001]* ZAPs are given in Fig. 1a, b and c, respectively. Notice that in Fig. 1a and c, spots corresponding *to* $0\,k\,0$: $k=2n+1$ and *00l*: $l=2n+1$ are observed because of multiple scattering of the diffracted beams.

Taking into account the information obtained from the SAED, we fitted the XRPD patterns and refined the unit-cell parameters using the JANA2000 program [13]. Notice that the c parameter doubling observed from the SAED is not obvious from the XRPD patterns. This would suggest that the structural features involved in

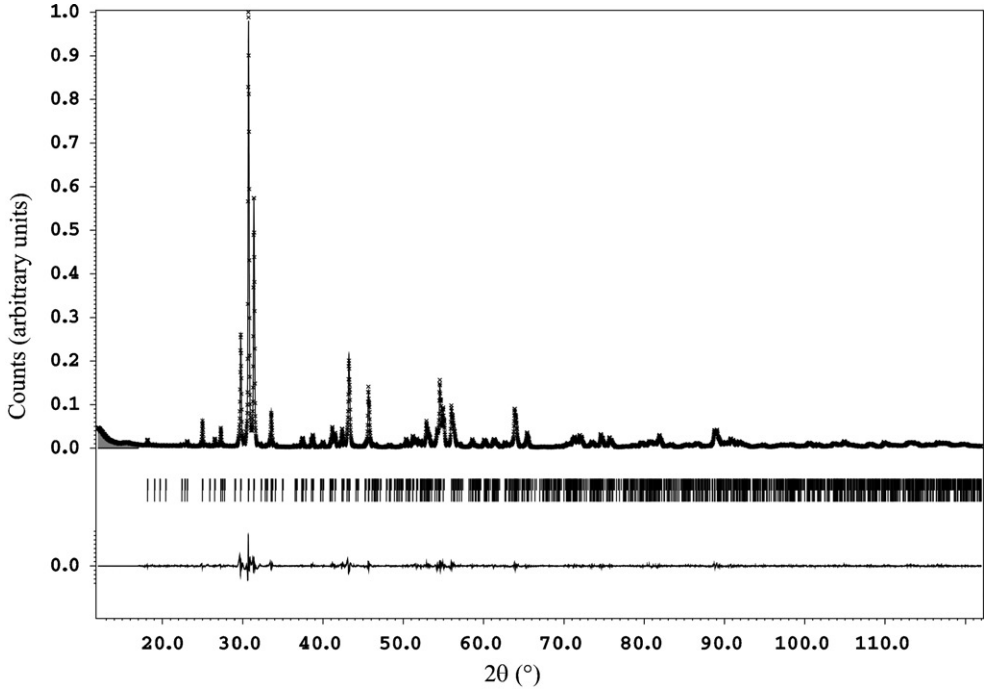

Fig. 2. Final observed, calculated and difference plots for the XRPD Rietveld refinement of La_2RuO_5. The set of tick marks represents the reflection associated to La_2RuO_5.

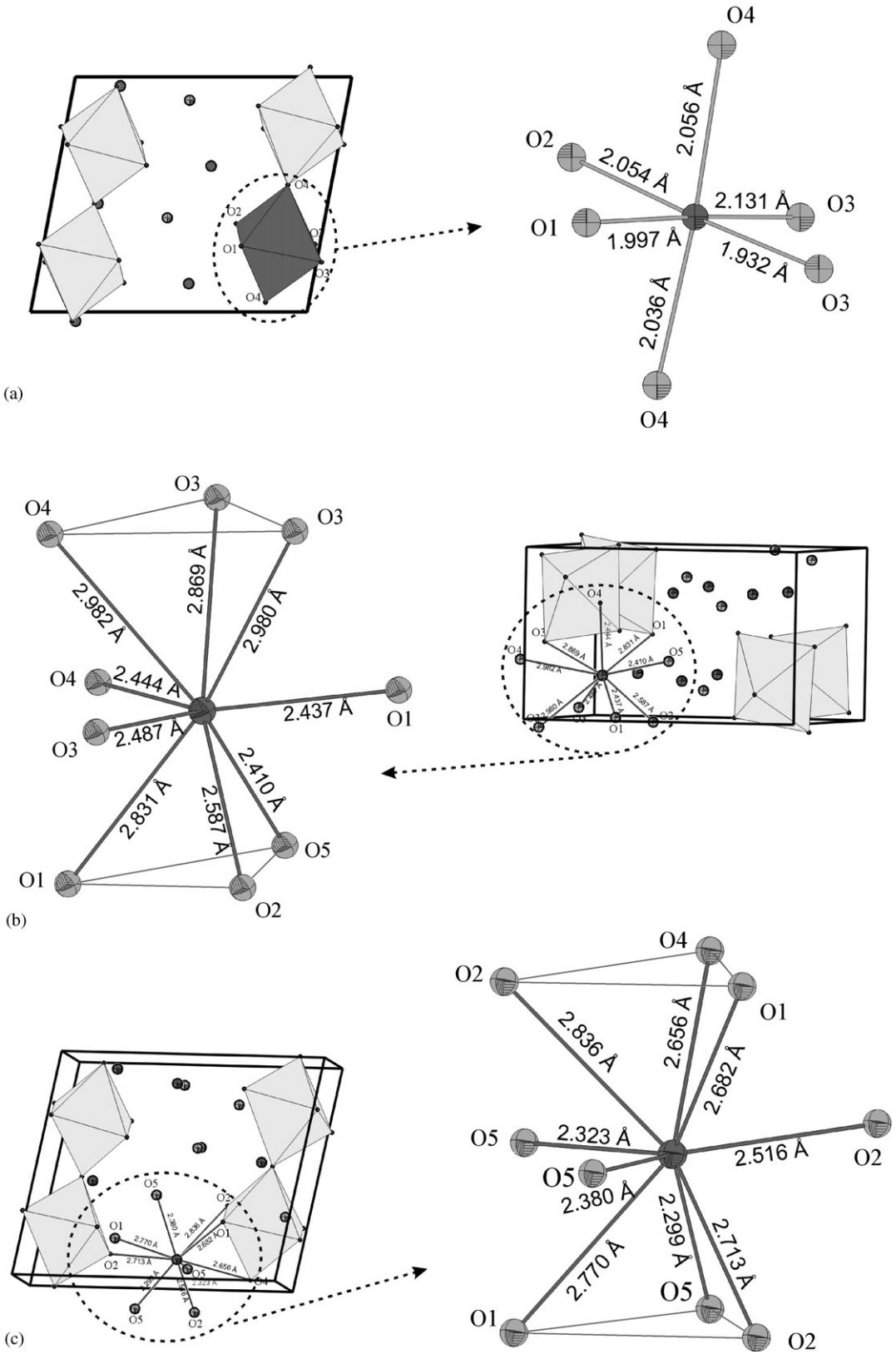

Fig. 3. Coordination shell around the (a) Ru, (b) La(1), and (c) La(2) cationic positions.

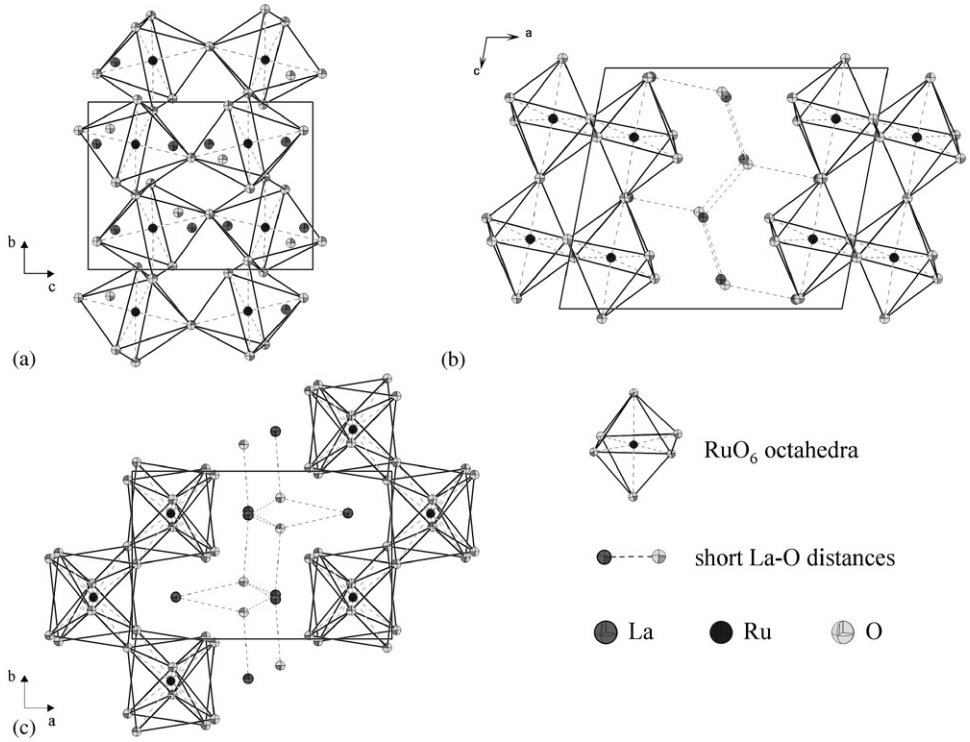

Fig. 4. Projection of the structure along the directions: (a) [100], (b) [010], and (c) [001]. The radii of the spheres used to represent the atomic positions correspond to the isotropic thermal parameters.

this doubling might involve light scattering atoms, i.e., oxygen.

4. Structure determination

The integrated peak intensities were extracted from the XRPD whole pattern fitting and the Patterson map was calculated with the JANA2000 program. The deconvolution of the Patterson map allowed us to find a first atomic position that was assigned to the atom with the strongest scattering factor, i.e., La. This atomic position was then used as a starting model for the Rietveld analysis. Two supplementary atomic positions (firstly assigned to La atoms) were then found through Fourier difference syntheses. After refinement of the atomic positions (U_{iso} fixed to 0.01), the R_F reliability factor reached a value close to 7.2%. The three determined atomic positions were all located on a 4*e* Wyckoff site. From the viewpoint of the approximate chemical composition of $La_2Ru_1O_5$ ($Z=4$), it was clear that these three positions corresponded to two La sites and one Ru site. The refinement of the isotropic thermal factors showed that one of them was significantly higher for one of the atomic positions and so we assigned this position to the Ru atom.

At this stage of the structural determination, the R_F reliability factor was close to 6% and the fit between the experimental and the calculated diffraction patterns look good to the eye ($R_p \sim 12\%$ and $\chi^2 \sim 11$). Additional Fourier difference syntheses were performed to find the position of the oxygen atoms by selecting peaks in the Fourier map corresponding to atomic positions located in the first coordination shell of the Ru atom, i.e., with Ru–O distances close to 2 Å. Four oxygen positions, corresponding to the four strongest maxima, were then located. The refinement of these oxygen positions (U_{iso} fixed to 0.01) significantly improved the reliability factors ($R_F = 3.7\%$, $Rp = 8.7\%$ and $\chi^2 = 4.4$). Finally, in light of the chemical composition, a fifth oxygen atomic position independent of the first Ru coordination shell was found and refined ($R_F = 2.7\%$, $R_{wp} = 10.8\%$ and $\chi^2 = 3.5$).

The results of the Rietveld refinement indicated some abnormally short O–O distances (less than 2.7 Å) resulting in an exaggerated deformation of the oxygen environment of the Ru atom (notably for the square plane of the RuO_6 octahedra). Four O–O soft distances constraints (O–O equal to 2.8 ± 0.05 Å) were then added. A last refinement was performed by introducing a common U_{iso} thermal factor for the position of the oxygen atoms, this resulted in the final atomic coordinates and thermal factors displayed in Table 1. Selected

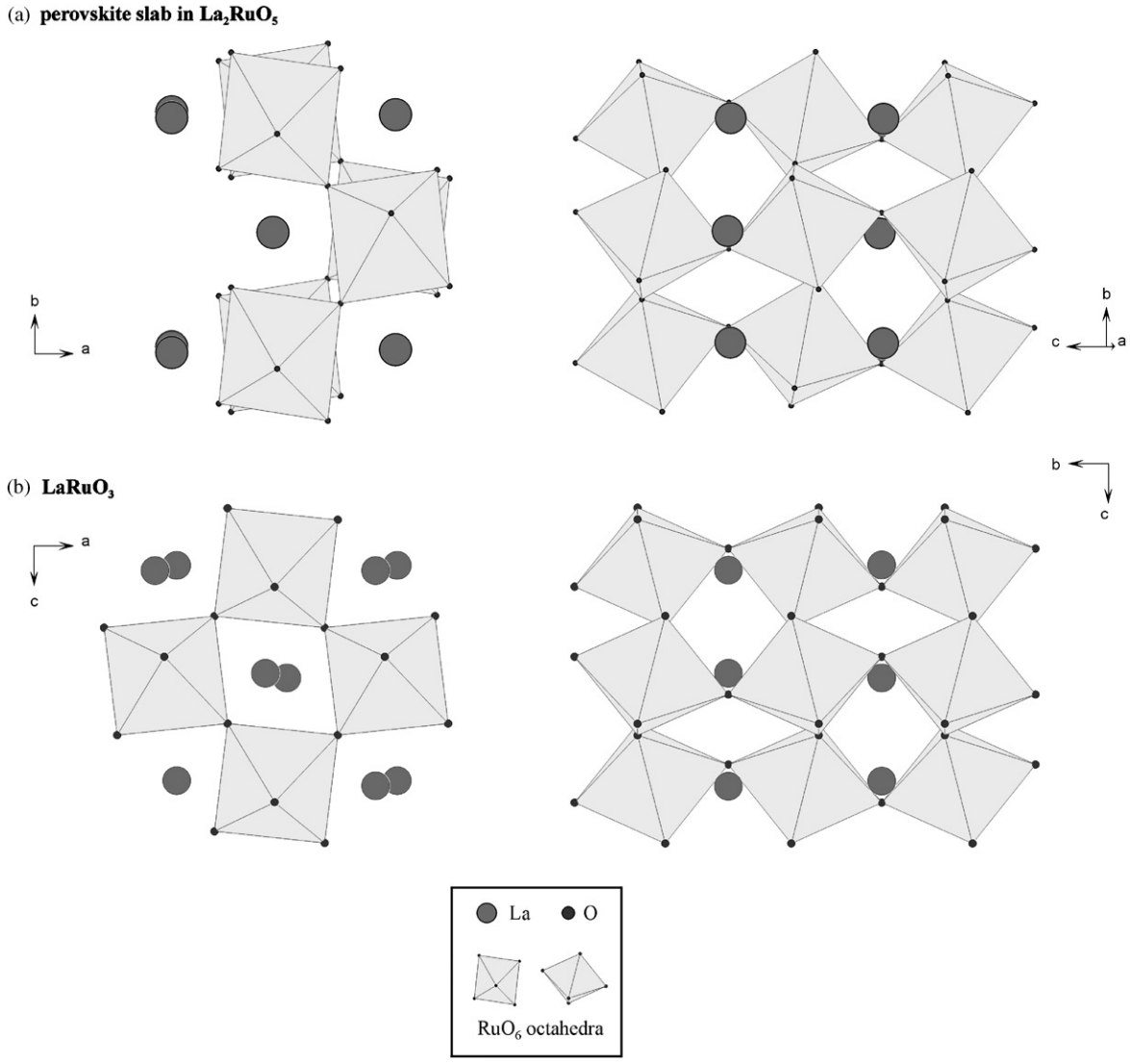

Fig. 5. Comparison of the tilt systems in (a) the perovskite slab of La_2RuO_5 and in (b) the $LaRuO_3$ perovskite.

inter-atomic distances and angles are given in Table 2. Using the program VaList [14], bond valence calculation gives estimated valences for La(1), La(2) and Ru of +2.8, +3.44 and +3.53 respectively. Fig. 2 shows the measured, calculated and difference diagrams obtained for the final Rietveld refinement of the XRPD patterns.

5. Results and discussion

Fig. 3 shows the coordination shell around the Ru, La(1) and La(2) atomic positions. From the XRPD refinements results, the Ru atom appears to be located in the center of its oxygen octahedral environment with distances ranging from 1.93(2) to 2.13(2) Å. The O–Ru–O angles (see Table 2) range from ~82° to ~95°, which indicates a slight distortion. The oxygen environments of La(1) and La(2), with nine oxygen atoms located within a 3 Å limit, can be described as disturbed tricapped trigonal prisms (Fig. 3b and c). In both cases, these nine oxygen atoms can be separated into two groups, four corresponding to short La–O distances ranging between ~2.3 and ~2.5 Å (three in the equatorial plane) and five to longer La–O distances ranging from ~2.6 to ~3.0 Å. The La(2) located within the $[LaO]_\infty$ slab (see below) exhibits three very short La(2)–O(5) distances (around 2.33 Å); however, considering the particular geometry of this slab, we could not expect to obtain distances longer than 2.4 Å.

The projections of the structure along the [100], [010] and [001] directions are given in Fig. 4a, b and c, respectively. It can be described as an intergrowth structure made up of regular stacking along the [100] direction of a two octahedra thick $[LaRuO_4]_\infty$ zigzag

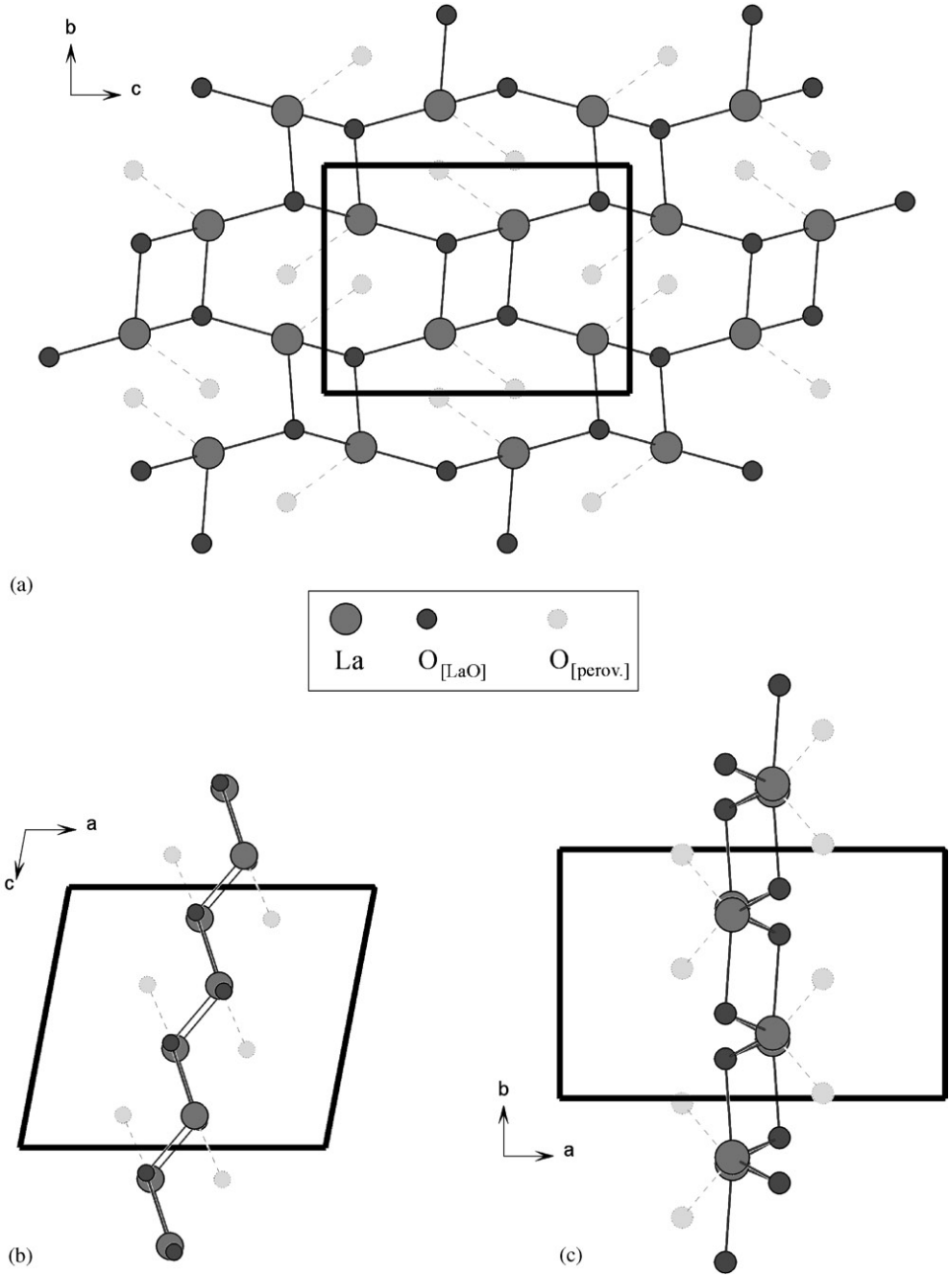

Fig. 6. Projection of the $[LaO]_\infty$ slab along the directions: (a) [100], (b) [010], and (c) [001].

perovskite slab and a $\sim$3.4 Å thick $[LaO]_\infty$ slab that expand infinitely in the (100) plane. The a unit-cell parameter thus corresponds to the summation of the thickness of these two slabs, i.e., $a \sim a_p\sqrt{2} + t_{[LaO]} \sim 5.8 + 3.4 \sim 9.2$ Å. The b and c unit-cell parameters derive directly from the perovskite slab and correspond to $b \sim a_p\sqrt{2} \sim 5.8$ Å and $c \sim 2a_p \sim 8.0$ Å.

The $[LaRuO_4]_\infty$ perovskite slab consists of a zigzag slab of RuO_6 octahedra running parallel to the [001] direction (Fig. 4c). In this slab, La(1) is present as in the $LaRuO_3$ [6–8,15] perovskite structure (Fig. 5). The observed tilting of the RuO_6 octahedra can be decomposed in three tilts with respect to the direction of a "basic" cubic perovskite (see Fig. 5a as an illustration). In reference to the Glazer notation of tilted octahedra in perovskite [16], the three tilts would correspond to a combination $a^-b^-c^-$ where alternate tilting of the octahedra in opposite directions are obtained along each direction of the cubic perovskite. The doubling of the c parameter, which is not obvious from the XRPD patterns, results from this tilting of the RuO_6 octahedra. For the sake of comparison, the perovskite phase of the

La–Ru–O system, which has the $GdFeO_3$-type structure, is represented in Fig. 5b. In La_2RuO_5, the $[LaRuO_4]_\infty$ perovskite slab exhibits a specific tilt system compared to the three tilts ($a^-a^-c^+$) system of the $LaRuO_3$ perovskite [15].

The $[LaO]_\infty$ slab, shown in Fig. 6, is a specific example of this structure. The projection along the [010] direction in Fig. 6b shows that the $[LaO]_\infty$ slab does not extend in the form of a plane layer but is bent with a sawtooth-like form. The projection along the [100] direction (Fig. 6a) shows the original net resulting from the 1–1 arrangement of O(5) oxygen and La(2) lanthanum atoms, where each lanthanum atom is connected to three oxygen atoms and vice versa. The connectivity scheme leads to a net that is built up by the regular alternation along both [010] and [001] directions of a small four-atom unit (diamond shape) and a large eight-atom unit. The connection with the perovskite slab is ensured by La(2)–O(2) bonds (represented by dashed lines in Fig. 6) alternately connected with the upper or the lower perovskite slab. Along the [100] direction, two O(2) oxygen (one above and one below) are facing the cavity formed by the large eight-atom units and thus minimizing the O–O electrostatic repulsion. Actually, the configuration of this slab is better understood from the viewpoint of the O(5) oxygen atoms' environments. In addition to the three O(5)–La(2) bonds, O(5) has a fourth shortest O(5)–La(1) bond with the La(1) atoms of the perovskite slab which results in a La_4 tetrahedral coordination for the O(5) atomic position. O_2La_6 units made up of two OLa_4 tetrahedra by edge-sharing are linked through corner-sharing in the (100) plane as represented in Fig. 7. These La_4 tetrahedral sites have an hexagonal close-packed arrangement in the (100) plane, where half of them are occupied by an O(5) atom resulting in a $[La_2O]_\infty$ composition. Such OLa_4 tetrahedra assembly can also be observed in α-La_2O_3 [17] or in some other compounds within the La–Ru–O system [1,2,5]; however, the connection between these tetrahedra is different from the one observed in La_2RuO_5.

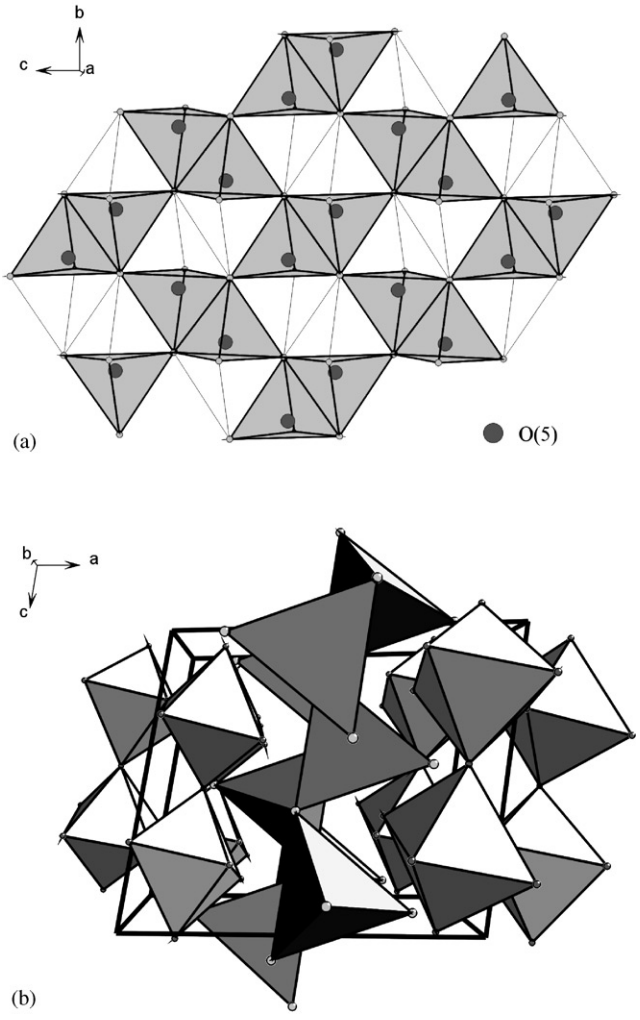

Fig. 7. Views of the La_4 tetrahedral coordination for the O(5) atomic position. (a) The La_4 tetrahedral sites are single out. They have an hexagonal close packed arrangement where half of them are occupied by a O(5) atom resulting in a $[La_2O]_\infty$ composition. (b) In this perspective view, the crystal structure of La_2RuO_5 can be seen as composed of a slab of corner sharing RuO_6 octahedra and a slab of corner-sharing O_2La_6 tetrahedral-based units.

6. Conclusion

The structure of the new oxide, La_2RuO_5, was solved by the combination of SAED and XRPD. The phase crystallizes in a monoclinic cell ($a=9.1878(2)$ Å, $b=5.8313(2)$ Å, $c=7.9575(2)$ Å and $\beta=100.773(2)^\circ$) with the $P2_1/c$ (SG no. 14) space group. In related systems, compounds with the formulation L_2RuO_5 (where L is Pr, Nd, Sm, Gd or Tb) have already been reported [18], but these compounds have a different orthorhombic structure. The reported crystal structure is, to our knowledge, not only different from those already reported for the La–Ru–O system but appears to have no equivalent structure in oxides. This new structural type can be described as the regular stacking of a two octahedra thick $[LaRuO_4]_\infty$ zigzag perovskite slab and a $\sim$3.4 Å thick $[LaO]_\infty$ slab. In terms of polyhedra assembly, the crystal structure is composed of a slab of corner sharing RuO_6 octahedra and a slab of corner-sharing O_2La_6 tetrahedral-based units (see Fig. 7b).

The presence of an original $[LaO]_\infty$ slab is undoubtedly the key feature of the new structure. One may wonder if this particularity could be compared to the $[BiO]_\infty$ slab encountered in the so-called Aurivillius phases [19], i.e., if one can anticipate the existence of a series of compounds having the general formulation $(LaO)_2^{2+}(A_nB_nO_{3n+2})^{2-}$, where n represents the number of corner-sharing octahedral layers. This would certainly be interesting in terms of potential properties that

such layered compounds based on transition metal oxides might exhibit. This possibility makes sense if one considers the large number of intergrowth compounds, where the bulk of the structure is made of a perovskite slab whose thickness can be expanded depending on the chemical composition (Aurivillius-type and HTc superconductor phases are among them). Further investigations are needed to check this possibility and to confirm whether the crystal structure of La_2RuO_5 is a singularity or not.

Acknowledgments

The authors wish to thank Dr. C. Pithan (Institut für Festkörperforschung) at the Jülich Research Center in Germany for chemical analyses.

References

[1] P. Khalifah, Q. Huang, J.W. Lynn, R.W. Erwin, R.J. Cava, Mater. Res. Bull. 35 (2000) 1–7.
[2] P. Khalifah, D.M. Ho, Q. Huang, R.J. Cava, J. Solid State Chem. 165 (2002) 359–362.
[3] P. Khalifah, Q. Huang, D.M. Huang, D.M. Ho, H.W. Zandbergen, R.J. Cava, J. Solid State Chem. 155 (2000) 189–197.
[4] F.A. Cotton, C.E. Rice, J. Solid State Chem. 24 (1978) 359–365.
[5] F.A. Cotton, C.E. Rice, J. Solid State Chem. 25 (1978) 137–142.
[6] R.J. Bouchard, J.F. Weiher, J. Solid State Chem. 4 (1972) 80–86.
[7] F.M. da Costa, R. Greatrex, N.N. Greenwood, J. Solid State Chem. 20 (1977) 381–389.
[8] C. Mallika, O.M. Sreedharan, J. Less-Common Metals 162 (1990) 51–60.
[9] F. Abraham, J. Trehoux, D. Thomas, J. Solid State Chem. 32 (1980) 151–160.
[10] F. Abraham, J. Trehoux, D. Thomas, Mater. Res. Bull. 12 (1977) 43–52.
[11] A. Bencan, 'Synthesis and characterization of lanthanum ruthenates', Ph.D.Thesis, Faculty of Chemistry and Chemical Technology, University of Ljubljana, 2002.
[12] P.E. Werner, L. Eriksson, M. Westdahl, J. Appl. Crystallogr. 18 (1985) 367–370.
[13] V. Petricek, M. Dusek, The Crystallographic Computing System JANA2000, Institute of Physics, Academy of Sciences of the Czech Republic, Praha, 2000.
[14] A.S. Wills, I.D. Brown, VaList, CEA, fft://ftp.ill.fr/pub/dif/valisty/, France, 1999.
[15] H. Kobayashi, M. Nagata, R. Kanno, Y. Kawamoto, Mater. Res. Bull. 29 (1994) 1271–1280.
[16] A.M. Glazer, Acta Crystallogr. B 28 (1972) 3384–3392.
[17] P. Aldebert, J.P. Traverse, Mater. Res. Bull. 14 (1979) 303–323.
[18] G. Cao, S. McCall, Z.X. Zhou, C.S. Alexander, J.E. Crow, Phys. Rev. B 63 (2001) 144 427.
[19] B. Aurivillius, Arkiv. Kemi 1 (1949) 463–480, 499–512.